Eur. J. Mech. B/Fluids 18 (1999) 739–756

Direct numerical simulation of turbulent mixing of a passive scalar in pipe flow

G. Brethouwer *, B.J. Boersma, M.B.J.M. Pourquié, F.T.M. Nieuwstadt

Delft University of Technology, Laboratory for Aero- and Hydro-dynamics, 2628 AL Rotterdamseweg 145, Delft, The Netherlands

(Received 27 January 1998; revised 7 September 1998; accepted 21 October 1998)

Abstract – Turbulent mixing of a passive scalar in fully developed turbulent pipe flow has been investigated by means of a Direct Numerical Simulation (DNS). The scalar is released from a point source located on the centreline of the pipe. The domain size of the concentration field has been chosen large enough to capture the different stages of turbulent mixing. Results are presented for mean concentration profiles, turbulent fluxes, concentration fluctuations, probability density functions and higher-order moments. To validate the numerical simulations the results are compared with experimental data on mixing in grid-turbulence that have been reported in the literature. The agreement between the experimental measurements and the computations is satisfactory. We have also considered the Probability Density Function (PDF). For small diffusion times and positions not on the plume centreline, our results lead to a PDF of an exponential form with a large peak at zero concentration. When the diffusion time increases, the PDF shifts from a exponential to a more Gaussian form. © Elsevier, Paris

DNS / turbulent mixing / pipe flow

1. Introduction

One of the main characteristics of turbulence is its efficient mixing of flow properties and additives. Turbulent mixing plays a role in various industrial and environmental flows. Examples are flow processes related to flames, fuel injection in engines, chemical reactors, stirred vessels but also dispersion of air pollution. Without mixing, many of these processes would be impossible. For instance, for a fast chemical reaction to take place rapid mixing is required to bring the reactive species in contact with each other on a molecular level. In order to understand or model these flows and processes, one must be able to predict the influence of turbulence on the mixing of scalars. Mixing takes place on all turbulent length and time scales. On the one hand, the large scales control the rate of spreading of a scalar across the flow. Information on this macro mixing can be provided by the mean concentration. On the other hand, the microscales are relevant when one considers mixing on a molecular level. Knowledge of this micro mixing requires detailed information on the statistics of concentration fluctuations, e.g. in terms of its Probability Density Function (PDF).

Because of its importance turbulent mixing has been a topic of much experimental and numerical research. In the past years a considerable amount of work has been done on developing models for mixing. Examples are PDF-models that are capable of describing microscale mixing in turbulent flows with or without chemical reactions. For a review of these models we may refer to Libby and Williams [1], Pope [2] and Fox [3]. When models become more elaborate and produce more detailed information on turbulent mixing, it is necessary to validate the results and to check the modelling assumptions which are made. The experimental measurements and numerical simulations that have been used for this purpose, have thus far been mainly restricted to mixing in homogeneous turbulence, with and without chemical reactions [4–7]. Turbulent mixing in shear flows

* Correspondence and reprints

has been less extensively investigated. However, in many applications turbulence is not homogeneous and thus data on mixing in turbulent shear flows are of interest. Therefore, we aim to consider here the latter subject.

As mentioned before the study of turbulent mixing processes requires detailed information on the spatial and time development of the concentration field. Such detailed information is usually very difficult to obtain experimentally. Numerical simulation of turbulence, in particular Direct Numerical Simulation (DNS), has evolved up to the point where we can use this technique with confidence to study the dispersion of admixtures in a turbulent flow. A DNS has the advantage that no modelling assumptions are necessary if the Schmidt number is not too large. Previous DNS studies on turbulent mixing have been carried out by Rogers et al. [8], Mell et al. [9] and Juneja and Pope [10]. These studies have been limited to homogeneous turbulence.

In the present study we will consider the DNS of mixing in inhomogeneous shear flow. For this we consider the release of a passive scalar from a small point source in the centre of a fully developed turbulent pipe flow. We have selected this flow geometry because results from a previous DNS [11] are available to us. This study has shown by means of careful comparison with experimental data that a realistic simulation of turbulence in a fully developed turbulent pipe flow can be obtained. Therefore, we select this numerical simulation as point of departure. Here we will concentrate on a spatially developing, passive concentration field, i.e. no chemical reaction takes place and the scalar does not influence the turbulent flow. The main objectives are to obtain more detailed information on the mixing process near the source and to investigate if a DNS is a useful tool for studying turbulent mixing in shear flows. To this end, results will be compared with experimental measurements on turbulent mixing in grid turbulence previously reported in literature. Not only the mean concentration will be considered but also second and higher-order moments and the PDF's of the concentration fluctuations.

The outline of the paper is as follows. In the next section the numerical method will be explained. Then the results will be presented for the mean concentration, turbulent concentration fluctuations and probability density functions of the concentration. Where possible, the results will be compared with available experimental data.

2. Numerical techniques and details of the computation

In a direct numerical simulation one considers the numerical solution of the full incompressible Navier-Stokes equations. For this case, where we consider the flow in a pipe, the equations have been formulated in cylindrical coordinates. The equations are discretised on a three-dimensional staggered grid by a finite volume method. For the discretization technique we use a centred scheme with second-order accuracy. For further details we refer to Eggels et al. [11].

Simultaneously with the equations that describe the turbulent flow motions, we also solve an advection–diffusion equation for a passive scalar. For the solution of this equation, a different numerical scheme is used. The radial advection term of the advection–diffusion equation is discretised with the standard second-order centred scheme. The advection terms in axial and tangential direction are discretised with a Total Variation Diminishing (TVD) scheme (see [12]). This is done because in these directions the cell Reynolds number defined as $Re = Udx/\nu$ with dx the grid spacing, is considerably greater than two. In this case, a second-order central scheme will produce non-physical oscillations which may lead to negative concentrations. Therefore we decided to use a TVD scheme which preserves monotonicity. This means that a local minimum does not decrease and a local maximum does not increase. The advantage of TVD schemes above other methods is that

it is accurate and a well established and well tested method which is computationally not to expensive for a DNS, see Vreugdenhil and Koren [13] and Zijlema and Wesseling [14]. The result of this scheme is that the concentration will never exceed the maximum concentration which is the source concentration and never go below the minimum concentration which in this case is zero. In other words the concentration will be always positive.

We should note here that a TVD scheme is only strictly monotonicity preserving in one dimension. However, in our three dimensional case the TVD scheme did not cause any significant negative concentrations. The upwind TVD scheme that we use is based on a limiter. This limiter screens the concentration field and decides which numerical scheme will be used for the interpolation of the concentration $c_{i+1/2}$ needed for the computation of the fluxes on the boundaries of the cells in the finite volume formulation. This decision is made depending on how smooth the concentration field is. In smooth parts of the concentration field a higher-order scheme is used and in non-smooth parts, where a higher order scheme may cause oscillations, a first-order scheme is applied. For instance, in extrema of the concentration field a first-order upwind scheme is used. Several of these limiters are available [12]. Here, we have chosen for the following limiter [15]:

$$
\begin{aligned}
c_{i+1/2} &= c_i + \frac{1}{2}\phi(r_{i+1/2})(c_i - c_{i-1}),\\
r_{i+1/2} &= \frac{c_{i+1} - c_i}{c_i - c_{i-1}},\\
\phi(r) &= \max\left(0, \min\left(2r, \min\left(\frac{1}{3} + \frac{2}{3}r, 2\right)\right)\right)
\end{aligned}
$$

because of its accuracy. The points needed for the interpolation of the concentration $c_{i+1/2}$ are taken at the upwind side. The interpolation results in a scheme which is a combination of a first-order upwind scheme and a correction to it to increase the accuracy.

For the computation of the flow field we apply periodic boundary conditions in the axial direction. The domain length of the flow field in this direction is $5D$ with D the pipe diameter. This domain length is determined by computational limitations. However, it is too short for an adequate simulation of the spatially developing concentration field. Therefore, we have put three periodic flow fields after each other to get a total domain length of $15D$ for the computation of the concentration field. The boundary conditions for the concentration are zero flux through the wall, a Dirichlet boundary condition at the inflow and a Neumann boundary condition at the outflow.

For the time integration of the advective terms a second order four stage Jameson scheme [12] is used and for the diffusive terms a second-order Adams–Bashforth scheme. For derivatives of the diffusive terms in the angular direction the implicit Crank–Nicholson scheme is applied. The velocity is corrected each time step by a pressure correction method in order to satisfy mass conservation. The number of grid points in radial, tangential and axial direction is $96 \times 128 \times (3 \times 256)$, respectively. The grid spacing used in the present study is the same as used by Eggels et al. [11]. The mean grid width near the wall equals 4.9 wall units whereas $\pi\eta^*$ with η the Kolmogorov length scale, equals 5.0 wall units. The Batchelor length scale which is smallest length scale of the scalar field, is equal to the Kolmogorov length scale because the Schmidt number equals one. Hence, the resolution is sufficient to resolve the smallest length scales, see for more details Eggels et al. [11].

At the inflow the scalar is prescribed in the form of a concentration profile with a Gaussian shape centred at the pipe axis. The standard deviation of this source is $8.5 \cdot 10^{-3} D$ which is comparable to the Kolmogorov

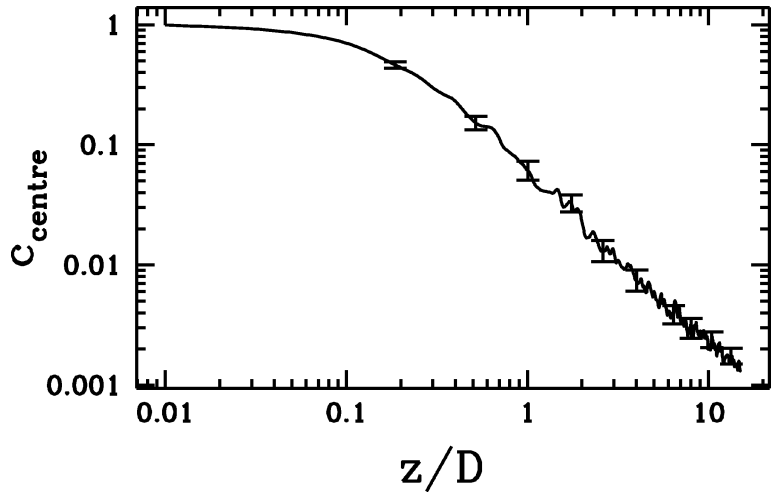

Figure 1. The mean centreline concentration as function of the axial distance to the source.

length-scale at the centre of the pipe and equal to two grid-spacings in radial direction. The Schmidt number is taken equal to one and the Reynolds number of the flow based on the mean velocity and the pipe diameter is 5300 which is the same Reynolds number used in the study of Eggels et al. [11]. The simulations are run for 2.5 time scales $t^* = D/u_*$ with u_* the shear stress velocity, before the data-analysis of the concentration field is started. The total time during which concentration data are sampled, measures 8 time scales t^* and during this period eighty nearly independent concentration data fields separated by an equal time period $0.1t^*$ [11] are stored for statistical analysis. The computations are run on a CRAY-C90. The complete run took approximately 400 CPU hours.

3. Results

The results for the mean velocity profiles and the turbulence statistics as obtained from our simulation are identical to those obtained by Eggels et al. [11]. Therefore, we will restrict ourselves here to only a presentation of the scalar dispersion results. In the next subsections various statistics of the concentration are presented and discussed.

3.1. Mean concentration

In *figure 1* the axial development of the mean centreline concentration is shown. In *figure 1* z/D is the non-dimensional axial distance to the source. The error bars show the interval in which the true mean centreline concentration lies with 90% confidence. These confidence limits have been determined based on the computed rms values at the centreline and the known number of statistical independent data (eighty). The results show that the confidence interval is equal to ± 0.2 times the mean centreline concentration. The variations in the curve fall in general within this error range and therefore should be attributed to statistical noise.

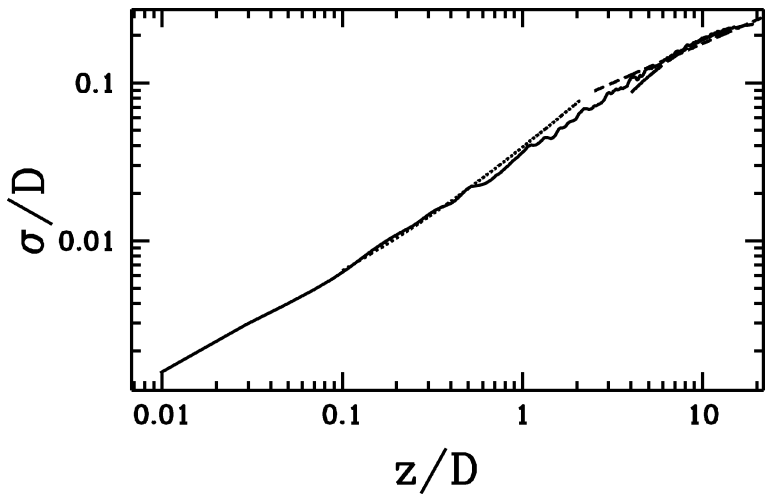

Figure 2. The dimensionless standard deviation in radial direction as function of the axial distance to the source. Solid line: simulations, dots: turbulent convection and molecular diffusion (I + II), short dashes: turbulent diffusion (III), long dashes: gradient transport model.

Figure 2 shows the standard deviation of the spreading of the mean concentration σ in radial direction as a function of downstream distance. It is defined by

$$\sigma^2 = \frac{1}{2}\frac{\int_0^\infty r^3 \overline{c}\, dr}{\int_0^\infty r\overline{c}\, dr}.$$

The standard deviation is made dimensionless with the pipe diameter and is corrected for the finite source size, i.e. $\sqrt{\sigma^2 - \sigma_0^2}$ is plotted with σ_0 the standard deviation of the source which is equal to $8.5 \cdot 10^{-3} D$. The solid line in *figure 2* denotes the calculation. If we can neglect the effect of the finite source size, three different stages can be distinguished in the evolution of a concentration plume in a stationary and homogeneous turbulent flow at high Reynolds number [16]. These stages are

I	molecular diffusion	$t \ll D_{\mathrm{mol}}/\overline{u'u'}$,	$\sigma^2 = 2D_{\mathrm{mol}}t$,
II	turbulent convection	$D_{\mathrm{mol}}/\overline{u'u'} \ll t \ll t_L$,	$\sigma^2 = \overline{u'u'}t^2$,
III	turbulent diffusion	$t \gg t_L$,	$\sigma^2 = 2\overline{u'u'}t_L t$,

where t is the diffusion time, D_{mol} the molecular diffusion coefficient, u' the Lagrangian velocity fluctuation and t_L the Lagrangian time scale. The expressions on the far right give in each region the growth rate of the standard deviation σ as a function of diffusion time.

In region I which is very close to the source, molecular diffusion dominates. As soon as the diffusion time exceeds the time scale of molecular diffusion, the dispersion process becomes dominated by turbulence. At first for short times, when turbulent motions are fully correlated, the standard deviation grows linearly in time. When turbulence decorrelates for larger diffusion times, the standard deviation is given by $\sigma \propto \sqrt{t}$. This occurs when the diffusion time is larger than the Lagrangian time scale. In our simulations this time scale in the centre of the pipe, is approximately $0.06D/u_*$ where u_* is the friction velocity. For U_c being the mean velocity at the centre of the pipe, we find that at $z = 1.1D$ the mean axial convection time z/U_c becomes equal to the Lagrangian time scale. This means that for $z \ll 1.1D$ the plume is in its first or second stage and for $z \gg 1.1D$ the plume is in the third stage of turbulent diffusion.

In *figure 2* lines are plotted which represent the expressions for σ in the three regions. The expressions for σ in the molecular diffusion stage (I) and the turbulent convection stage (II) are added together (line I+II) because at low Reynolds number and short diffusion time molecular diffusion and turbulent convection contribute about equal to the spreading of the plume. To evaluate the expressions given above, we need the Lagrangian velocity fluctuation and the diffusion time. For the Lagrangian velocity fluctuation we take the radial rms velocity at the pipe centre and for the diffusion time the mean axial convection time z/U_c. We find that line I + II agrees reasonable well with the calculations for $z \ll 1.1D$ as expected.

Line III gives the spreading of the plume in the final stage of turbulent diffusion. For large diffusion times line III should give a reasonable approximation to the computed σ. However, at large diffusion times the scalar has entered the non-homogeneous wall region. In addition the concentration is reflected from the wall due to the no-flux boundary condition. This causes differences with the expression given above for $t \gg t_L$ which in principle is only valid for homogeneous unbounded turbulence. Hence, the expression for σ in the turbulent diffusion stage is not very appropriate and leads to a poor agreement with the computational value of σ as can be seen in *figure 2*. A better description for the development of the plume at large diffusion times is given by a gradient transport model in which the turbulent concentration flux is modelled as $-\overline{u'c'} = D_T \partial\overline{c}/\partial r$ where D_T is the turbulent diffusion coefficient given as a function of radial position. The gradient transport model assumes that the length scale of the scalar field is larger than the length scale of the turbulence and this is only true for large diffusion times. For short diffusion times the gradient transport model therefore fails. In *figure 2* a comparison is given between the calculated standard deviation and the result according to the gradient transport model. The mean concentration according to the gradient transport model is calculated by solving the Reynolds averaged advection–diffusion equation for fully developed pipe flow given by

$$\frac{\partial \overline{w}\,\overline{c}}{\partial z} = -\frac{1}{r}\frac{\partial r\overline{u'c'}}{\partial r} + D_{\mathrm{mol}}\frac{1}{r}\frac{\partial}{\partial r}\left(r\frac{\partial \overline{c}}{\partial r}\right)$$

where the turbulent flux $\overline{u'c'}$ is closed by means of the gradient transport hypothesis mentioned above. The mean axial velocity profile, $\overline{w}(r)$ is taken equal to the velocity profile obtained from our simulation. The turbulent diffusion coefficient D_T is calculated with the aid of $Sc = \nu_T/D_T = 0.9$ (this value is chosen based on the best fit to the data) where ν_T, the turbulent viscosity, is also determined from our DNS data. The agreement between the gradient transport model and our simulation results is satisfactory.

Figure 3 shows the mean concentration profiles scaled with the centreline value at various axial positions. The error bars have the same meaning as in *figure 1*. The mean concentration profiles are given as a function of the radial distance scaled with the standard deviation of the mean concentration at that distance. For comparison a Gaussian curve is also drawn in *figure 3*. At $z = 3D$ and $z = 9D$ the mean concentration profiles are nearly Gaussian with small statistical scatter. At $z = 13D$, the scalar profile has reached the wall and a significant deviation from the Gaussian form occurs. The mean concentration profile at $z = 13D$ has been calculated with the gradient transport model which is described above. The result is also plotted in *figure 3* for comparison. The mean concentration profile predicted by the gradient transport and the calculated mean concentration profile agree well.

For a comparison of our simulation results with experimental data we are limited to the many experiments that have been done on turbulent mixing in grid-generated homogeneous turbulence. This type of turbulence may taken to be reasonably representative for the centre region of the turbulent pipe flow. Nevertheless, it should be mentioned that a comparison with experimental measurements is not straightforward because of differences in Schmidt number, Reynolds number, source size and source geometries which all have a large influence on the statistics of mixing. Therefore differences between the experiments and our simulations are likely to occur.

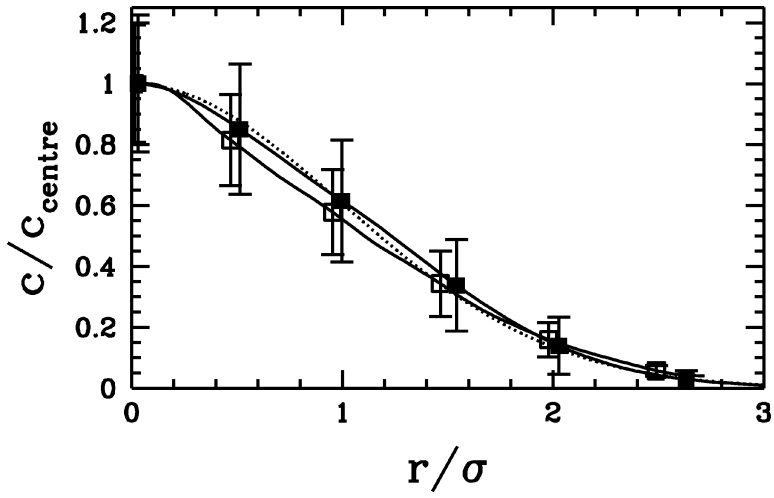

(b)

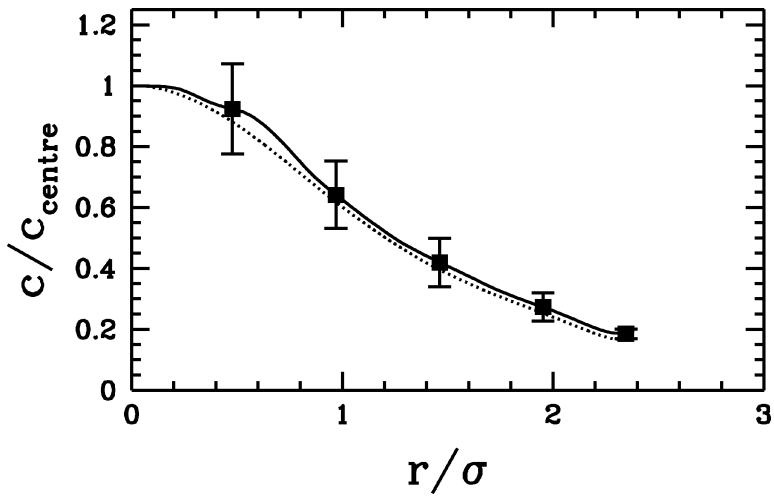

(a)

Figure 3. The radial mean concentration profiles. (a) The concentration profiles at $z = 3D$ (■) and $z = 9D$ (□), dotted line is the Gaussian distribution. (b) The concentration profile at $z = 13D$ (■), dotted line is the gradient transport model. The concentration is scaled with the centreline concentration and the radial distance is scaled with σ.

In almost all experiments on mixing in grid turbulence, a line source has been used instead of a point source like in our simulations. For instance, Warhaft [16], Li and Bilger [5], Stapountzis et al. [6], Sawford and Sullivan [17] and Veeravalli and Warhaft [18] all have investigated turbulent mixing behind a line source in grid-generated turbulence. They found that the cross-stream concentration profiles have a Gaussian form. Brown and Bilger [4] and Nakamura et al. [19] investigated turbulent mixing behind a point source in grid-generated turbulence. They also found Gaussian radial mean concentration profiles. These experimental results for the mean cross-stream concentration profile are in agreement with our results for short diffusion times ($z/D < 9$) which also show a Gaussian concentration profile. At larger distances from the source we have found deviations from the Gaussian profile in our simulation because the scalar enters the wall region and this causes significant deviations from the Gaussian profile.

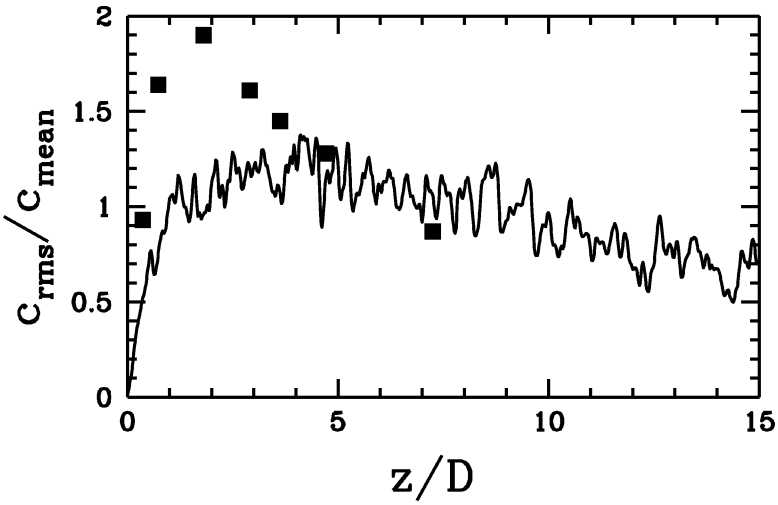

Figure 4. The centreline rms of the concentration scaled with the centreline mean concentration as function of the axial distance to the source, drawn line: simulations and (■): model of Thomson [20].

3.2. Concentration fluctuations

In this section we consider the statistics of the concentration fluctuations. First, we show in *figure 4* the rms of the concentration fluctuations at the centre of the pipe as a function of the axial distance from the source. The rms of the concentration fluctuations is normalised with the local mean concentration. The data show significant scatter due to statistical error. Nevertheless, some trends can be observed. At the source the rms is zero by definition because a constant concentration profile is prescribed at $z = 0$. Next, the relative intensity of the fluctuations increases and reaches at $z/D \simeq 5$ its maximum value which lies between 1.0 and 1.4. After this the relative intensity decreases to a value between 0.5 and 0.8 at the end of the domain. Also shown are the predictions given by the model of Thomson [20] which applies to a comparable flow situation. This is a stochastic model which describes the motions of particle pairs in homogeneous and isotropic turbulence without molecular diffusion at infinite Reynolds number. Thomson's model predicts larger relative intensities close to the source than our simulation results and seems to lead to lower values far from the source. This difference is probably the result of the difference in Reynolds number, i.e. the low Reynolds number in our simulations versus the infinite Reynolds number assumed in the model of Thomson.

An extension to Thomson's model has been discussed by Borgas and Sawford [21]. They added molecular diffusion and viscous effects to the two-particle Lagrangian model. According to Borgas and Sawford [21] the effect of molecular diffusion and viscosity is to decrease the maximum relative intensity and to increase the relative intensity for large diffusion times. Hence it is plausible that incorporating molecular diffusion and viscous effects improves the agreement between the Lagrangian model and our simulations.

Experiments on turbulent mixing in grid turbulence (i.e. [5,6,16–18] show a maximum relative intensity of concentration fluctuations on the centreline with a value between 0.8 and 1.2 which is close to our DNS data. In all these experiments a line source was used. Brown and Bilger [4] have used a point source and found a maximum value of 0.8. These latter authors have used a point source which is at least an order of magnitude larger than the Kolmogorov length scale. In our simulations the point source is comparable in size to the Kolmogorov length scale. It is likely that this explain the larger maximum relative intensity found in our simulations in comparison to the value obtained by Brown and Bilger [4]. After the maximum value has been reached, the relative intensity according to these experiments decreases further monotonically.

Fackrell and Robins [22] have investigated turbulent mixing in a boundary layer by means of dispersion from point sources with different sizes. They found a maximum relative intensity of 1.3 for the largest source and 5 for the smallest source. The increase of the maximum relative intensity with decreasing source size has been confirmed by Thomson [20] with his stochastic model for the motion of particle pairs in isotropic turbulence that we have mentioned above. This points out the importance of the source size for the relative intensity of the concentration fluctuations, especially close to the source. Further downstream the influence of the source size becomes less according to the experiments of Fackrell and Robins [22].

Not only the size of the source is important but also whether the source geometry is a line or a point source. When a point source is used a plume can meander in two dimensions but when a line source is used the plume can only meander in one dimension. Hence a larger relative intensity is to be expected for the case of a point source. This is confirmed by Borgas and Sawford [21] and according to their model the difference in the maximum relative intensity behind a line and point source can be as large as a factor of two. This perhaps explains the somewhat larger relative intensity that we find in comparison with the results of Sawford and Sullivan [17], Veeravalli and Warhaft [18], Stapountzis et al. [6], Warhaft [16], Li and Bilger [5]. On the whole it can nevertheless be concluded that the calculated relative intensity seems to be in reasonable accordance with the above mentioned experimental measurements.

Figure 5 shows the radial profiles of the rms of the concentration fluctuations at different axial positions. The rms values are scaled with the centreline rms and the radial distance is scaled with the standard deviation of the mean concentration. Note that the profile of the concentration fluctuations is much wider than the profile of the mean concentration shown in *figure 3*. Also shown in *figure 5* are the experimental data of Brown and Bilger [4] obtained for the mixing behind a point source in homogeneous turbulence. Their measurements were taken at different positions downstream of the source in the turbulent diffusive range. Our results for large diffusion times, i.e. $z > 3D$, show good agreement with these experimental data. For short diffusion times ($z = 0.2D$) the rms profiles for the simulation results show a off-centre peak which is not observed in the experimental data. It should be mentioned that the DNS data at the largest axial distances are not statistically converged and therefore have not been shown here.

According to Thomson [20] three different stages can be distinguished in the development of the rms profiles. These stages do not coincide with the stages mentioned in Section 3.1 because the processes involved in evolution of mean concentration and of the concentration fluctuations are not the same.

In the first stage, the plume makes meandering movements which are small compared to the size of the plume. Therefore the greatest rms values appears on the place where the concentration gradient is greatest. This is confirmed in *figure 5* where the profile of the rms close to the source shows an off-centre maximum.

In the second stage the relative intensity of concentration fluctuations becomes large and the place of the maximum rms moves towards the centre. According to Thomson [20] this stage (at least for mixing behind a line source at an infinite Reynolds number) occurs when the relative intensity becomes greater than one. *Figure 5* shows the rms profiles at $z = 3D$ and $z = 5D$ and at these axial positions the maximum of the rms is on the centreline or close to it.

In the third stage meandering becomes less important and mixing takes place by turbulent motions smaller than the plume itself. The rms is then determined by local processes. Thomson [20] argues that in this third stage the off-centre peak reappears near the place where the concentration gradient is greatest. For further explanation of the above mentioned phenomena we refer to Sawford and Sullivan [17] and Chatwin and Sullivan [23]. The reappearance of the off-centre peak at large diffusion times could not be confirmed by our simulation results because at large diffusion times the DNS data show too much scatter. Furthermore, at large diffusion times we cannot neglect the influence of the pipe wall.

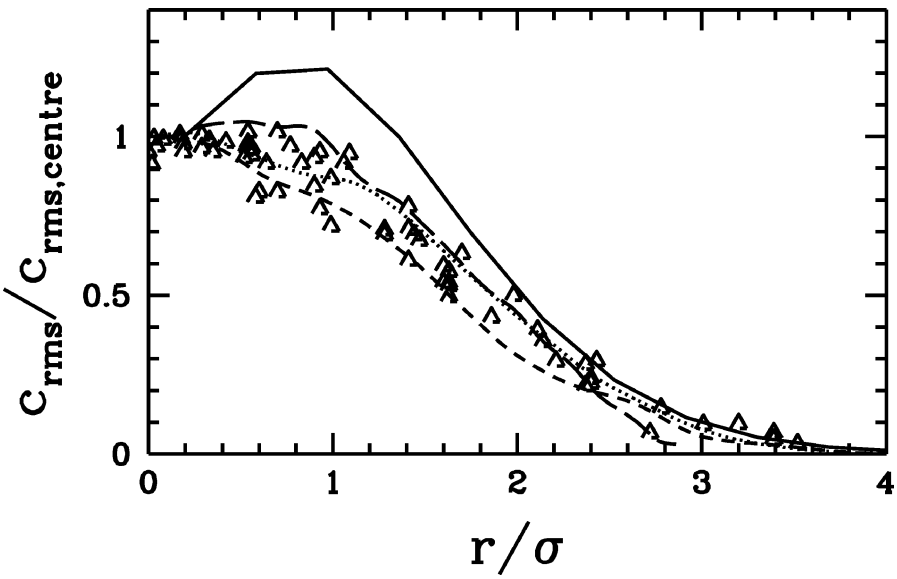

Figure 5. The radial rms profiles of the concentration at $z = 0.2D$ (solid), $z = 3D$ (dots), $z = 5D$ (short dashes), $z = 8.3D$ (long dashes), markers are the results of Brown and Bilger [4]. The rms is scaled with the centreline rms and the radial distance is scaled with σ.

Stapountzis et al. [6], Sawford and Sullivan [17] and Warhaft [16] found in their experiments an off-centre peak in the rms of the concentration fluctuations close to the source in agreement with our results shown in *figure 5*. Further downstream they found that the peak moves towards the centreline and the profiles of the rms approach a Gaussian form also in agreement with our results. In some experiments [16,17] an off-centre rms peak reappears at positions far downstream the source. However, Nakamura et al. [19] found a Gaussian rms profile far downstream the source.

In *figure 6* we show the standard deviation of the $\overline{c'c'}(r)$ profile normalised with the standard deviation of the mean concentration as a function of the distance from the source. The data show quite some scatter but it is nevertheless clear from *figure 6* that the relative standard deviation decreases as the distance from the source increases. Close to the source the relative standard deviation has a value between 0.95 and 1.0 and decreases to a value between 0.8 and 0.85 at the end of the domain. According to the experiments of Warhaft [16], performed in grid-turbulence, the standard deviation of $\overline{c'c'}$ normalised with the standard deviation of the mean concentration is nearly one. This is close to our results for short diffusion times. At large diffusion times the relative standard deviation is influenced by the wall and decreases.

3.3. Concentration fluxes

In *figure 7* we show the profiles of the turbulent flux in radial direction as a function of r/σ at various distances from the source. In the same *figure* the experimental results of Brown and Bilger [4] are given. The turbulent flux is presented in the form of a correlation coefficient, i.e. normalised with the rms of the concentration fluctuations and the rms of the radial velocity fluctuations. The profiles of this correlation coefficient show a maximum at about $r/\sigma = 1$ which is approximately the place where the mean concentration gradient is largest. The profiles at positions close to the source have a higher maximum than the profiles at positions further downstream. This is probably the result of the change in dynamics of mixing from turbulent convective transport to turbulent diffusive transport, which has been discussed already in Section 3.1. In the

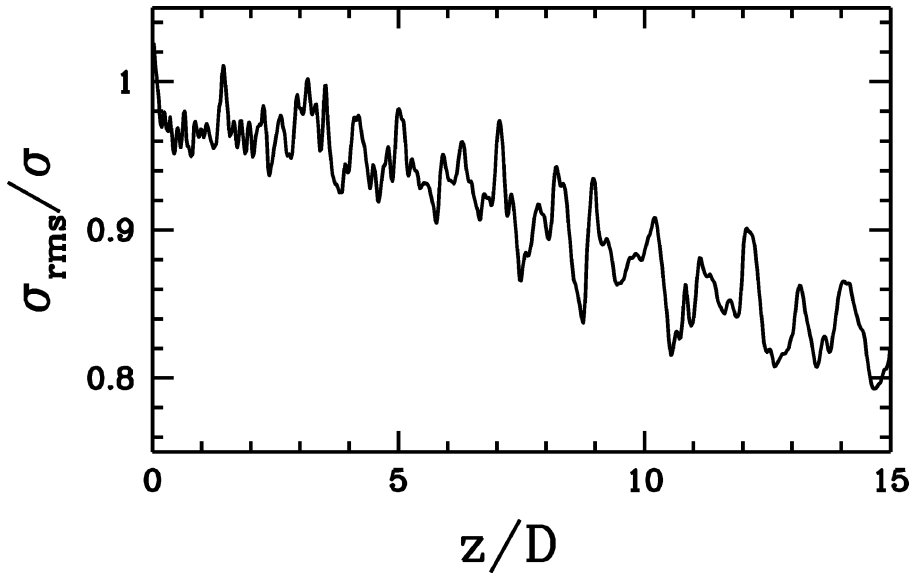

Figure 6. The standard deviation of $\overline{c'c'}$ scaled with σ.

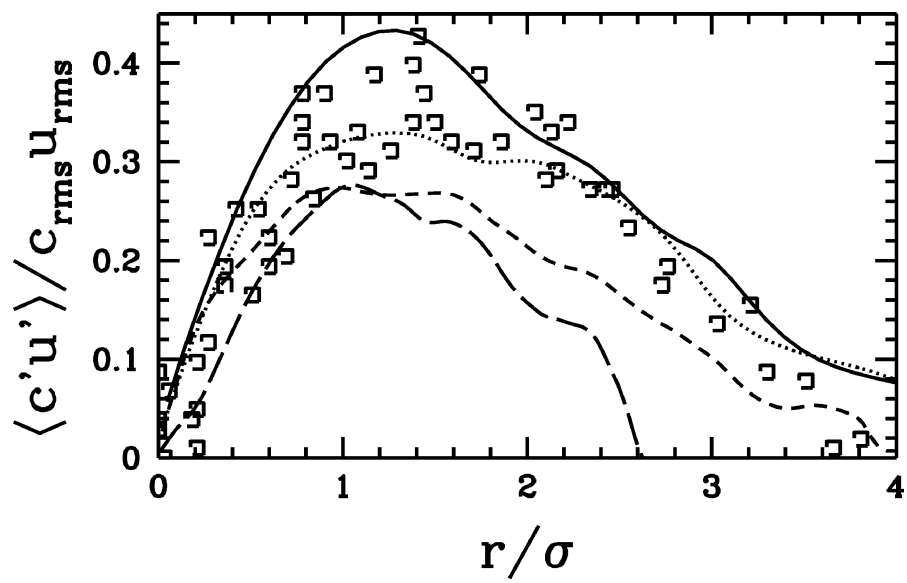

Figure 7. The radial profiles of $\overline{c'u'}/(c'_{rms}u'_{rms})$ at $z = 1.8D$ (solid), $z = 2.7D$ (dots), $z = 4.9D$ (short dashes), $z = 9.8D$ (long dashes), markers are the results of Brown and Bilger [4].

stage of turbulent convection the apparent turbulent diffusion coefficient grows in time and in the turbulent diffusive stage the turbulent diffusion coefficient reaches its asymptotic value.

In our simulations the maximum value for the turbulent flux is approximately 0.25 at large diffusion times, i.e. $z > 5D$ which is in the turbulent diffusive stage. This is somewhat lower than the asymptotic maximum value found by Brown and Bilger [4] which is approximately 0.35, see *figure 7*. The reason for this difference is most probably the influence of the wall on the turbulent flux and the difference in the Reynolds number between the experiments of Brown and Bilger [4] and our simulations. The influence of the wall is probably

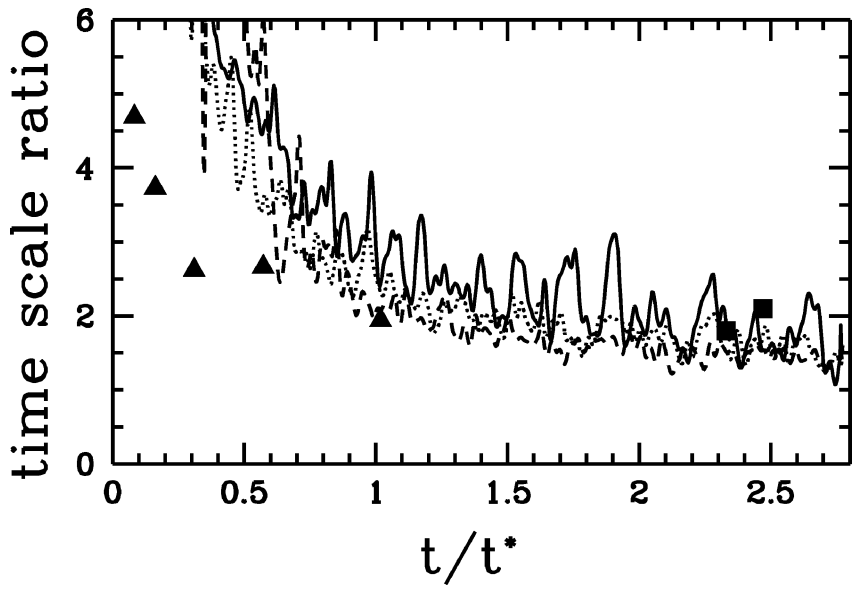

Figure 8. The time scale ratio of kinetic energy dissipation to the scalar dissipation $(\varepsilon_c/\overline{c'c'})/(\varepsilon/k)$ at $r = 0.10R$(solid), $r = 0.31R$ (dots) and $r = 0.625R$ (dashes). ■: results of Brown and Bilger [4], ▲: results of Li and Bilger [5].

also the explanation for the strong decrease of dimensionless turbulent flux at $r/\sigma > 2$ as the distance from the source increases.

3.4. Time scale

Next we consider the ratio of the time scale of kinetic energy dissipation to the time scale of the scalar dissipation given by $(\varepsilon_c/\overline{c'c'})/(\varepsilon/k)$ where ε_c is the dissipation of scalar fluctuations, ε the dissipation of turbulent kinetic energy and k the turbulent kinetic energy. This ratio of the two time scales is illustrated in *figure 8* as a function of t/t^* at three r/R positions. Here, t is the mean advection time $z/\overline{u}_{\text{axial}}$ and $t^* = k/\varepsilon$ is the turbulent time scale. The data show significant scatter, especially close to the centreline. Nevertheless, it appears that the time scale ratio decreases as the distance to the source increases and it approaches an asymptotic value of around 1.5.

Also shown in *figure 8* are the experimental measured values of the time scale ratio of Brown and Bilger [4] and Li and Bilger [5]. The time scale ratio estimated by Brown and Bilger and by Li and Bilger in the far field agree good with our results. Béguier et al. [24] measured the time scale ratio in different shear flows and found a value close to 2 for all flows. Close to the source Li and Bilger [5] measured lower values of the time scale ratio. The experiments of Warhaft and Lumley [25] suggest that the time scale ratio depends on the initial ratio of scalar length scale and turbulent length scale. Hence, the difference between our results and the results of Li and Bilger may be due to the different ratio of source size to turbulent length scale.

It should be also mentioned here that in commonly used closure models (see, e.g. [5,26] this time scale ratio is assumed to be a constant with a value usually taken equal to two. In comparison with our results such an assumption is clearly not correct.

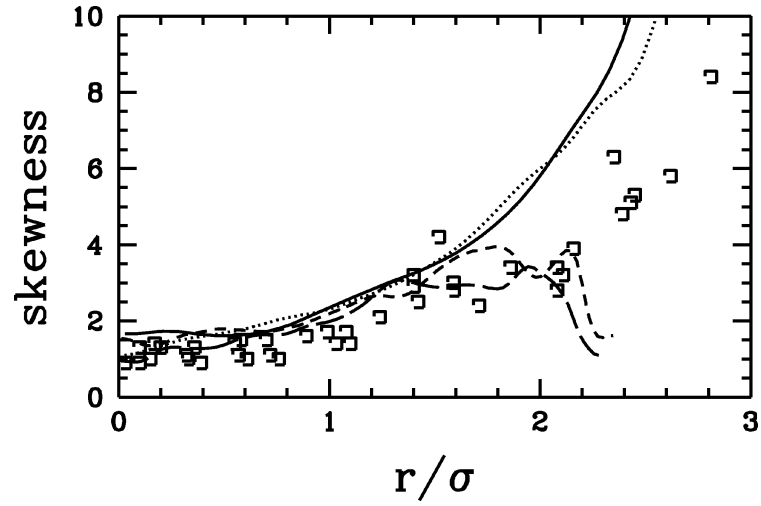

(a)

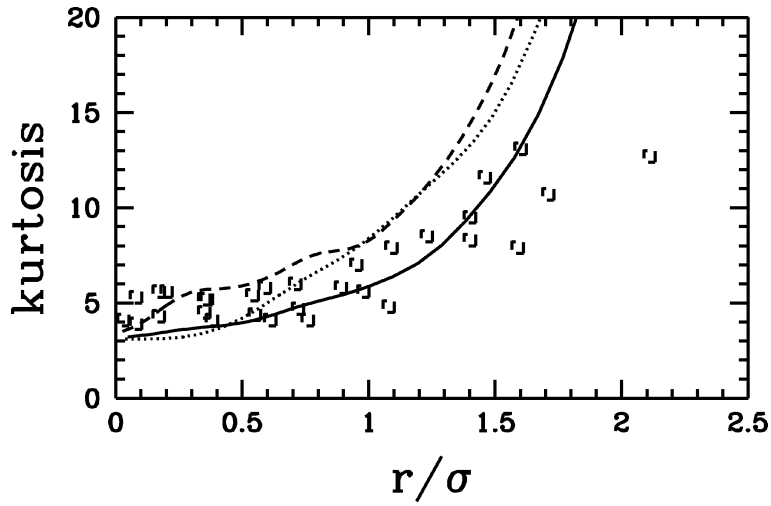

(b)

Figure 9. (a) The radial skewness profiles of the concentration fluctuations at $z = 3.1D$ (solid), $z = 3.5D$ (dots), $z = 12.2D$ (short dashes), $z = 13.2D$ (long dashes), markers are the results of Brown and Bilger [4]. (b) The radial kurtosis profiles of the concentration fluctuations at $z = 1.8D$ (solid), $z = 2.3D$ (dots), $z = 3.5D$ (short dashes), markers are the results of Brown and Bilger [4]. The radial distance is scaled with σ.

3.5. Higher-order moments and intermittency

In the present subsection we consider the higher-order moments of the concentration fluctuation c'.

Figure 9(a) shows the radial profiles of the skewness of the concentration at various axial positions where the skewness is defined by

$$Sk = \frac{\overline{c'^3}}{\overline{c'^2}^{3/2}}.$$

The radial distance is normalised with the radial standard deviation of the mean concentration profile. In *figure 9* the experimental data of Brown and Bilger [4] have been given also. At all positions the skewness is positive. This means that the PDF of the concentration fluctuations is asymmetric and is skewed towards larger concentrations. Only close to the source the skewness is negative (not shown). At $z = 3.3D$ the skewness increases as the radial distance increases. This is in agreement with the experiments of Li and Bilger [5] and Brown and Bilger [4], shown in the same *figure*. This means that the peak of probability density function shifts towards lower concentration as the radial distance increases. This may be the result of intermittency which we discuss further below. At $z = 3.3D$ the simulations predicts a somewhat larger skewness than the experimental data of Brown and Bilger [4] for radial distances larger than zero. At the centre the agreement between experiments and simulations is good. Going further downstream the skewness decreases, especially for $r/\sigma > 1.5$ which is probably due to the influence of the wall.

Figure 9(b) shows the radial profiles of the kurtosis of the concentration fluctuations in the region between $z = 1.8D$ and $3.5D$ where the kurtosis is defined by

$$Ku = \frac{\overline{c'^4}}{\overline{c'^2}^2}.$$

In the same *figure* we also give the experimental results of Brown and Bilger [4]. The radial position is normalised with the standard deviation of the mean concentration. At the centre of the pipe the kurtosis has a value somewhat higher than 3 which applies to a normal probability density distribution. With increasing radial distance the kurtosis increases and becomes much larger than three. These results indicate that the concentration does not have a normal distribution but instead has a distribution with a long tail. The tail becomes longer when the radial distance increases. The increase of the kurtosis with increasing radial distance is in agreement with the experiments of Li and Bilger [5] and Brown and Bilger [4]. Similarly as for the skewness, the reason for the increase of the kurtosis at large values of r/σ is most likely intermittency to be discussed below. On the whole, the agreement with the experiments of Brown and Bilger [4] is satisfactory.

In *figure 10* we present the intermittency on the centreline where the intermittency is defined as the fraction of time in which the concentration is non-zero. The concentration is regarded as zero if it is smaller than a

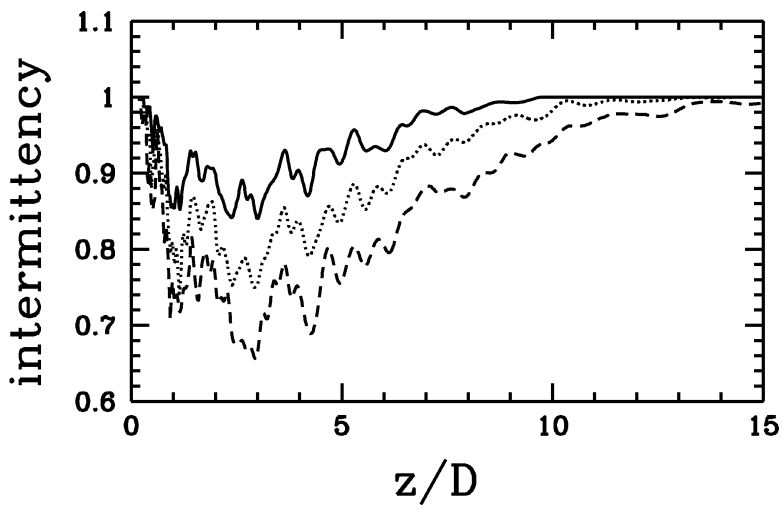

Figure 10. The centreline intermittency as function of the axial distance to the source. Solid is for a threshold value of 0.01, dots for 0.04 and dashes for 0.1.

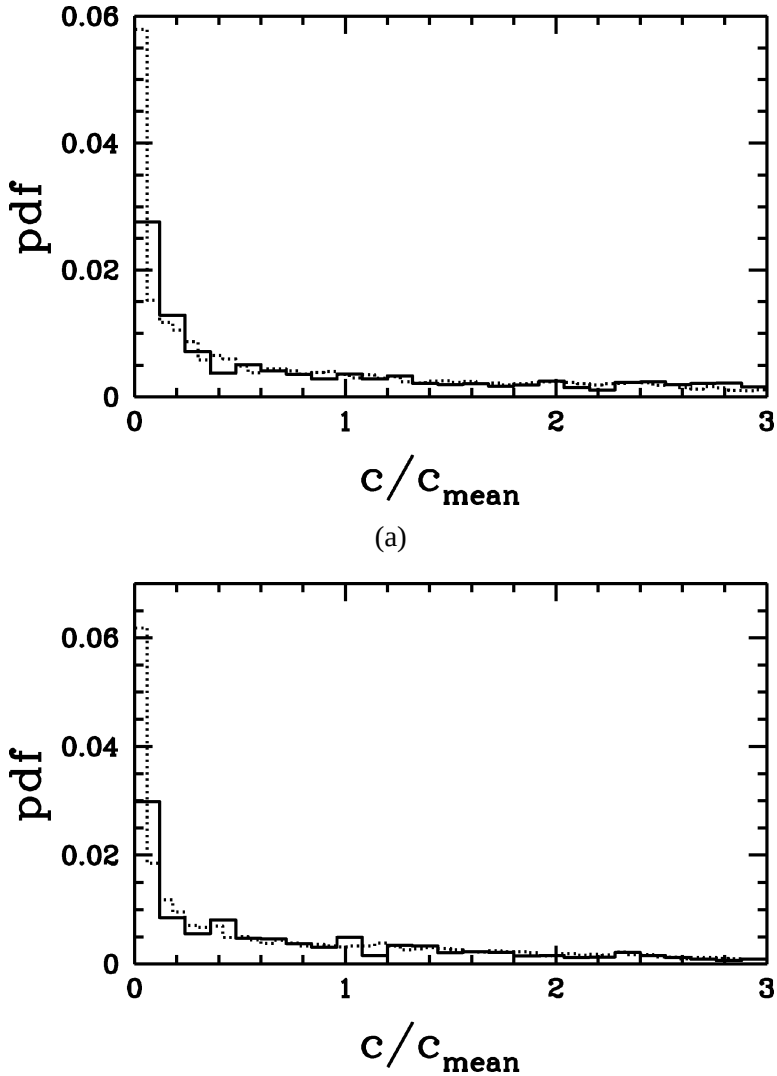

Figure 11. (a) The PDF of the concentration at $z = 1.6D$ at the centre (solid) and at $r = 0.37\sigma$ (dots). (b) The PDF of the concentration at $z = 3.1D$ at the centre (solid) and at $r = 0.33\sigma$ (dots).

certain threshold value. Here we have used three different threshold values, 0.01, 0.04 and 0.10 times the local mean concentration. The intermittency depends strongly on the threshold values for the concentration as can be seen in the *figure*. From *figure 10* it is clear that the intermittency first decreases as the distance to the source increases. This can be attributed to the meandering of the plume. After this the intermittency increases again and this can be attributed to turbulent mixing.

3.6. Probability density functions

In various models which describe the turbulent mixing process, use is made of a Probability Density Function (PDF) for the concentration. Therefore, it is useful to present PDF's for our simulations. In *figures 11* and *12* we

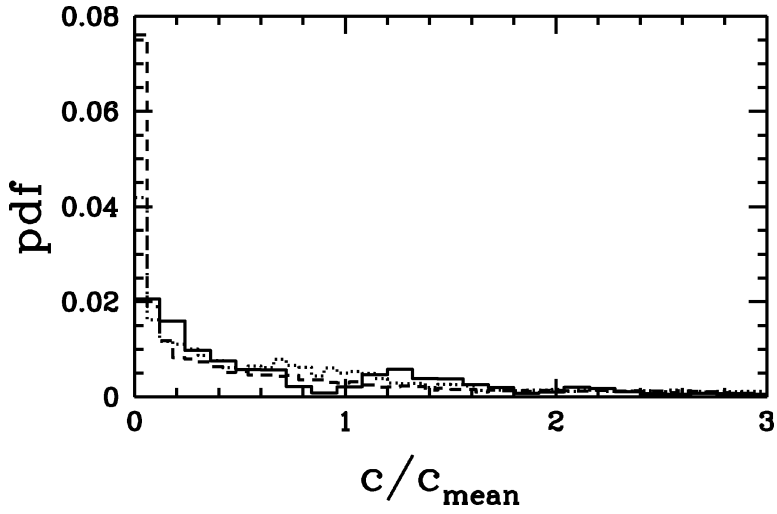

(a)

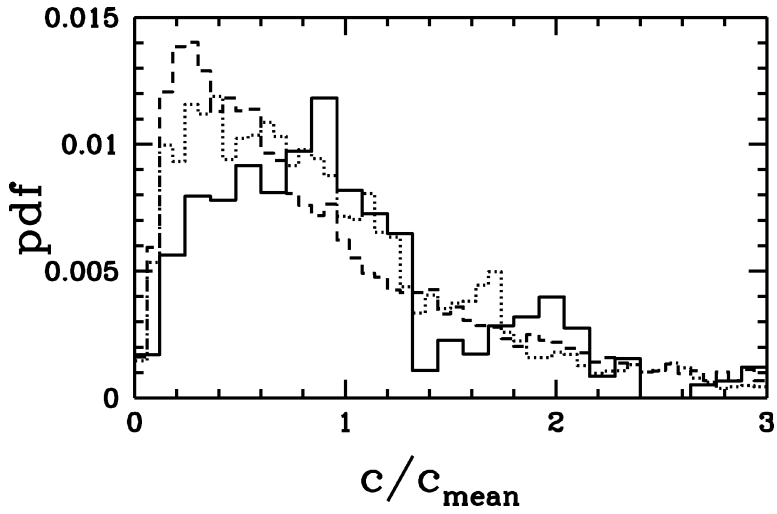

(b)

Figure 12. (a) The PDF of the concentration at $z = 6.3D$ at the centre (solid), at $r = 0.42\sigma$ (dots) and at $r = 1.0\sigma$ (dashes). (b) The PDF of the concentration at $z = 12.5D$ at the centre (solid), at $r = 0.36\sigma$ (dots) and at $r = 1.4\sigma$ (dashes).

show the PDF of the instantaneous concentration at different axial and radial positions where the concentration is scaled with the local mean concentration. The radial distance r^+ is scaled with the standard deviation of the mean concentration σ.

On the centreline the PDF's at $z = 1.6D$, $z = 3.1D$ and $z = 6.3D$ have an exponential form and the exponential shape becomes more pronounced as the radial distance to the centre increases. The exponential form of the PDF's implies that a value of zero concentration has a high probability. This means that the intermittency is significantly less than one at these positions, i.e. the concentration is mostly zero and becomes only non-zero when a blob of concentration passes by. This agrees with the trends observed for the skewness and kurtosis. Namely, we have found a positive skewness on the centreline and an increasing skewness and kurtosis for an increasing distance to the centre.

Going further downstream the value of the PDF at zero concentration decreases and according to *figure 12(b)* the peak value of the PDF at zero concentration disappears at $z = 12.5$. The decrease of the PDF at zero concentration is probably the result of mixing at the small scales, i.e. molecular diffusion. The results for the PDF's agree qualitatively with the experiments of Li and Bilger [5]. They found that when the distance to the centre increases the peak value of the PDF moves to zero concentration. They also found that the PDF on the centre changes gradually towards a normal distribution as the distance to the source increases and a the largest distance to the source they found that the PDF on the centre has a Gaussian form.

4. Conclusions

The turbulent mixing of a passive scalar emitted from a point source in fully developed turbulent pipe flow has been investigated by a direct numerical simulation. The point source is located at the centre of the pipe. The domain size is large enough to include the different stages of turbulent mixing, from turbulent convection to turbulent diffusion. Mean concentration profiles, rms profiles for the concentration fluctuations, probability density functions for the concentration and other statistical quantities are presented.

Experimental results for the same flow configuration are not available but where possible, a comparison is made with experimental data on mixing in grid turbulence. The data of our simulations sometimes show considerable scatter due to statistical noise, especially at large distances from the source, and this makes it difficult to compare our results with experimental data. Nevertheless, the following conclusion may be drawn.

The radial mean concentration profiles are Gaussian except at large diffusion times where deviations from the Gaussian form occur due to the presence of the wall. The radial rms profiles of concentration fluctuations show a off-centre peak near the source while further downstream this off-centre peak disappears. The rms profiles at large diffusion times agree reasonably well with the experimental results of Brown and Bilger [4]. The radial profiles of the normalised turbulent flux show a peak at $r/\sigma = 1$ which approaches an asymptotic value of about 0.25 at large diffusion times. This value is somewhat lower than the experimentally measured value of 0.35 by Brown and Bilger [4]. The PDF's determined at several radial and axial distances, have an exponential shape with a peak at zero concentration. This exponential shape becomes more pronounced as the distance to the centreline increases. Only at the largest distances from the source this exponential form of the PDF changes slowly towards a Gaussian form.

In general it may be concluded that in spite of statistical noise in our data the agreement between simulations and experiments is reasonably good. Consequently, a direct numerical simulation has been found to be a useful tool to study turbulent mixing processes in shear flows.

Acknowledgements

This project is supported by the Dutch research foundation FOM. We would like to thank the Dutch super computing foundation NCF for providing the computation time.

References

[1] Libby P.A., Williams F.A. (Eds), Turbulent Reacting Flows, Academic Press, London, 1994.
[2] Pope S.B., Lagrangian PDF methods for turbulent flows, Annu. Rev. Fluid Mech. 26 (1994) 23–63.
[3] Fox R.O., Computational methods for turbulent reacting flows in the chemical process industry, Rev. Inst. Franç. du Pétrole 51 (2) (1996) 215–243.

[4] Brown R.J., Bilger R.W., An experimental study of a reactive plume in grid turbulence, J. Fluid Mech. 312 (1996) 373–407.
[5] Li J.D., Bilger R.W., The diffusion of conserved and reactive scalars behind line sources in homogeneous turbulence, J. Fluid Mech. 318 (1996) 339–372.
[6] Stapountzis H., Sawford B.L., Hunt J.C.R., Britter R.E., Structure of the temperature field downwind of a line source in grid turbulence, J. Fluid Mech. 165 (1986) 401–424.
[7] Eswaran V., Pope S.B., Direct numerical simulations of the turbulent mixing of a passive scalar, Phys. Fluids 3 (1988) 506–520.
[8] Rogers M.M., Mansour N.N., Reynolds W.C., An algebraic model for the turbulent flux of a passive scalar, J. Fluid Mech. 203 (1989) 77–101.
[9] Mell W.E., Nilsen V., Kosály G., Riley J.J., Investigation of closure models for nonpremixed turbulent reacting flows, Phys. Fluids 6 (1994) 1331–1356.
[10] Juneja A., Pope S.B., A DNS study of turbulent mixing of two passive scalars, Phys. Fluids 8 (1996) 2161–2184.
[11] Eggels J.G.M., Unger F., Weiss M.H., Westerweel J., Adrian R.J., Friedrich R., Nieuwstadt F.T.M., Fully developed turbulent pipe flow: a comparison between direct numerical simulations and experiment, J. Fluid Mech. 268 (1994) 175–210.
[12] Hirsch C., Numerical Computations of Internal and External Flows, Wiley, New York, 1988.
[13] Vreugdenhil C.B. and Koren B., Numerical Methods for Advection-Diffusion Problems, Notes on Numerical Fluid Mechanics 45, Vieweg, Braunschweig, 1993.
[14] Zijlema M., Wesseling P., Higher-order flux-limiting schemes for the finite volume computation of incompressible flow, IJCFD 9 (1998) 89–109.
[15] Koren B., Robust upwind discretization method for advection, diffusion and source terms, in: Vreugdenhil C.B., Koren B. (Eds), Numerical Methods for Advection-Diffusion Problems, Notes on Numerical Fluid Mechanics 45, Vieweg, Braunschweig, 1993, pp. 117–138.
[16] Warhaft Z., The interference of thermal fields from line sources in grid turbulence, J. Fluid Mech. 144 (1984) 363–387.
[17] Sawford B.L., Sullivan P.J., A simple representation of a developing contaminant concentration field, J. Fluid Mech. 289 (1995) 141–157.
[18] Veeravalli S., Warhaft Z., Thermal dispersion from a line source in the shearless turbulence mixing layer, J. Fluid Mech. 216 (1990) 35–70.
[19] Nakamura I., Sakai Y., Miyata M., Diffusion of matter by a non-buoyant plume in grid-generated turbulence, J. Fluid Mech. 178 (1987) 379–403.
[20] Thomson D.J., A stochastic model for the motion of particle pairs in isotropic high-Reynolds-number turbulence, and its application to the problem of concentration variance, J. Fluid Mech. 210 (1990) 113–153.
[21] Borgas M.S., Sawford B.L., Molecular diffusion and viscous effects on concentration statistics in grid turbulence, J. Fluid Mech. 324 (1996) 25–44.
[22] Fackrell J.E., Robins A.G., Concentration fluctuations and fluxes in plumes from point sources in a turbulent boundary layer, J. Fluid Mech. 117 (1982) 1–26.
[23] Chatwin P.C., Sullivan P.J., A simple and unifying physical interpretation of scalar fluctuation measurements from many turbulent shear flows, J. Fluid Mech. 212 (1995) 533–556.
[24] Béguier C., Dekeyser I., Launder B.E., Ratio of scalar and velocity dissipation time scales in shear flow turbulence, Phys. Fluids 21 (1978) 307–315.
[25] Warhaft, Z., Lumley J.L., An experimental study of the decay of temperature fluctuations in grid-generated turbulence, J. Fluid Mech. 88 (1978) 659–684.
[26] Fox R.O., The spectral relaxation model of the scalar dissipation rate in homogeneous turbulence, Phys. Fluids 7 (1995) 1082–1094.